Title

Cytotoxicity of 2D engineered nanomaterials in pulmonary and corneal epithelium

Authors

Domanico, Morgan

Fukuto, Atsuhiko

Tran, Lisa M

et al.

Publication Date

2022-04-01

DOI

10.1016/j.impact.2022.100404

Peer reviewed

HHS Public Access

Author manuscript

NanoImpact. Author manuscript; available in PMC 2022 June 17.

Published in final edited form as:

NanoImpact. 2022 April ; 26: 100404. doi:10.1016/j.impact.2022.100404.

Cytotoxicity of 2D engineered nanomaterials in pulmonary and corneal epithelium

Morgan Domanico[a],

Atsuhiko Fukuto[c,d],

Lisa M. Tran[a],

Jessica-Miranda Bustamante[a],

Patricia C. Edwards[a],

Kent E. Pinkerton[a,b],

Sara M. Thomasy[c,e],

Laura S. Van Winkle[a,b,*]

[a]Center for Health and the Environment, University of California-Davis, Davis, CA, USA

[b]Department of Anatomy, Physiology and Cell Biology, School of Veterinary Medicine, University of California-Davis, Davis, CA, USA

[c]Department of Surgical and Radiological Sciences, School of Veterinary Medicine, University of California-Davis, Davis, CA, USA

[d]Department of Ophthalmology and Visual Sciences, Graduate School of Biomedical Sciences, Hiroshima University, Hiroshima, Japan

[e]Department of Ophthalmology & Vision Science, School of Medicine, University of California-Davis, Davis, CA, USA

Abstract

Two-dimensional (2D) engineered nanomaterials are widely used in consumer and industrial goods due to their unique chemical and physical characteristics. Engineered nanomaterials are

*Corresponding author at: Center for Health and the Environment, University of California-Davis, Davis, CA, USA. lsvanwinkle@ucdavis.edu (L.S. Van Winkle).

CRediT authorship contribution statement

Morgan Domanico: Formal analysis, Investigation, Writing – original draft, Writing – review & editing, Visualization. **Atsuhiko Fukuto:** Formal analysis, Investigation, Writing – original draft, Writing – review & editing. **Lisa M. Tran:** Formal analysis, Investigation, Writing – review & editing. **Jessica-Miranda Bustamante:** Methodology, Investigation, Writing – review & editing. **Patricia C. Edwards:** Methodology, Writing – review & editing, Project administration. **Kent E. Pinkerton:** Conceptualization, Methodology, Writing – review & editing, Funding acquisition. **Sara M. Thomasy:** Conceptualization, Methodology, Writing – review & editing, Supervision, Funding acquisition. **Laura S. Van Winkle:** Conceptualization, Methodology, Writing – review & editing, Supervision, Funding acquisition.

Declaration of Competing Interest

The authors declare the following financial interests/personal relationships which may be considered as potential competing interests:collaborator who supplied research consortium with nanomaterials is also editor-in-chief of Nanoimpact - Dr. Philip Demokritou.

Appendix A. Supplementary data

Supplementary data to this article can be found online at https://doi.org/10.1016/j.impact.2022.100404.

incredibly small and capable of being aerosolized during manufacturing, with the potential for biological interaction at first-contact sites such as the eye and lung. The unique properties of 2D nanomaterials that make them of interest to many industries may also cause toxicity towards epithelial cells. Using murine and human respiratory epithelial cell culture models, we tested the cytotoxicity of eight 2D engineered nanomaterials: graphene (110 nm), graphene oxide (2 um), graphene oxide (400 nm), reduced graphene oxide (2 um), reduced graphene oxide (400 nm), partially reduced graphene oxide (400 nm), molybdenum disulfide (400 nm), and hexagonal boron nitride (150 nm). Nongraphene nanomaterials were also tested in human corneal epithelial cells for ocular epithelial cytotoxicity. Hexagonal boron nitride was found to be cytotoxic in mouse tracheal, human alveolar, and human corneal epithelial cells. Hexagonal boron nitride was also tested for inhibition of wound healing in alveolar epithelial cells; no inhibition was seen at sub-cytotoxic doses. Nanomaterials should be considered with care before use, due to specific regional cytotoxicity that also varies by cell type. Supported by U01ES027288 and T32HL007013 and T32ES007059.

Graphical Abstract

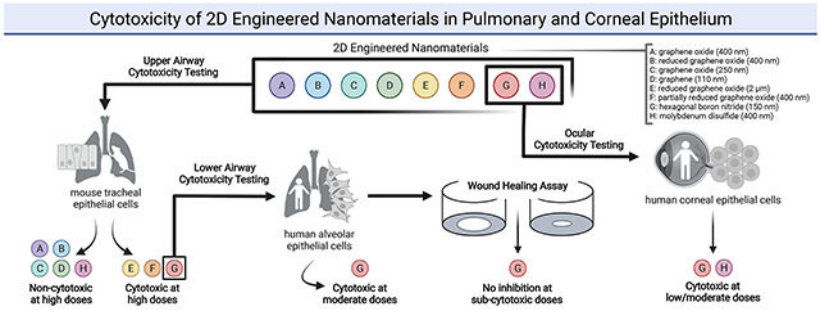

Keywords

2D engineered nanomaterials; Hexagonal boron nitride; Airway epithelial cells; Corneal epithelial cells; Nanotoxicity

1. Introduction

Two-dimensional (2D) nanomaterials are a subclass of engineered nanomaterials (ENMs) hallmarked by a single sheet of covalently bonded atoms, with a large surface area and intriguing chemical properties (Hu et al., 2019; Nath et al., 2019). These nanomaterials are widely incorporated in consumer products (Vance et al., 2015), and have unique properties with utility in electronics (Parlak et al., 2013), optical systems (Zhang et al., 2017), as well as mechanical and thermal industries (Nath et al., 2019).

We tested a subset of widely used 2D ENMs, including graphene, hexagonal boron nitride (hBN), and molybdenum disulfide (MoS_2). Graphene possesses a high degree of conductivity (Balandin, 2011; Chen et al., 2011; Chen et al., 2012), thermodynamic stability (Lui et al., 2009), and incredible intrinsic strength (Lee et al., 2008). Boron nitride-based nanomaterials are characterized by thermal stability and resistance to oxidation (L. H. Li

et al., 2014; Z. Liu et al., 2013), as well as low friction (Jiang et al., 2015). Hexagonal boron nitride is used as a lubricant (Jiang et al., 2015), corrosion inhibitor (Chilkoor et al., 2018), and cosmetic additive for luster (Fiume et al., 2015). Molybdenum disulfide (MoS_2) is an excellent semiconductor, lubricant, and industrial catalyst (Nardekar et al., 2020). The small size but high surface area of 2D ENMs also makes them of interest for drug delivery and other biomedical applications (Merlo et al., 2018; Şen et al., 2019) and can impact size-dependent reactivity and toxicity (Gatoo et al., 2014).

Exposure to ENMs can occur through biomedical, environmental, or occupational routes (Nath et al., 2019). Biomedical exposures are often controlled and better understood, but exposure to nanomaterials can also occur as transformation products in the environment, or as byproducts during occupational processes. Allied Market Research reports the use and manufacturing of carbon-based nanomaterials are projected to approximately double in future years, with the nanotechnology market value near tripling by 2030 (https://www.alliedmarketresearch.com/nanotechnology-in-energy-market), and there is concern about occupational inhalation exposure to nanomaterials during manufacturing processes (Arvidsson et al., 2013). Due to their very small size, nanomaterials can be inhaled as nanoparticles in aerosol form and deposited in the respiratory tract (Hoet et al., 2004; Oberdörster et al., 2005). Inhalation exposures to nanoparticles are of particular concern as the lungs are the site of initial contact, possessing a large surface area for deposition to occur and have the potential for particle accumulation if not properly cleared, as well as having potential for direct contact with the circulatory system (Li et al., 2010) due to an extremely thin air-to-blood tissue barrier. Exposure to a similar class of ENMs, carbon nanotubes, has been associated with lung tumor progression in a mouse model (Sargent et al., 2014).

The epithelium that lines the respiratory tract is vulnerable to interaction with deposited nanoparticles which can result in toxicity (Li et al., 2010). Primary mouse tracheal epithelial cell culture was chosen to model the upper airway, which is well-conserved among mammalian species. The use of primary mouse tracheal epithelium facilitates evaluation of cellular differentiation for the various cell types found in the upper-airway epithelium — ciliated, mucous, and basal cells — allowing for diverse multi-cell responses to these nanomaterials. For further testing of select nanomaterials, immortalized human alveolar epithelial cells were cultured to represent the lower lung epithelium where smaller nanomaterials would be capable of depositing. Our endpoints included cytotoxicity as well as wound healing, because particles can have negative impacts other than cell death, including inhibition of epithelial regeneration and repair following acute injury.

In an occupational exposure to aerosolized nanomaterials, the eye is likely to receive a similar exposure as through an inhalation route (Yah et al., 2012). Air pollutants are known to have direct contact with the ocular surface (Chang and Yang, 2020). The cornea is the outermost layer of the eye, in direct contact with the external environment, and is crucial for the protection of delicate internal ocular structures. Nanomaterials are often used in an occupational setting with unknown risks regarding their ocular toxicity. Thus, this data is critical for risk assessment to provide appropriate guidance regarding safety measures to limit ocular exposure to aerosolized nanomaterials. We sought to address this data gap

regarding ocular toxicity of 2D nanomaterials by also testing in corneal epithelial cell culture models.

Using corneal and lung epithelial cell culture models, we tested the cytotoxicity of eight 2D engineered nanomaterials: graphene oxide (400 nm), reduced graphene oxide (400 nm), graphene oxide (250 nm), graphene (110 nm), reduced graphene oxide (2 um), partially reduced graphene oxide (400 nm), hBN (150 nm) and MoS_2 (400 nm). Initial *in vitro* results prompted further testing of hBN for cytotoxicity and cellular migration (wound healing) in human alveolar epithelial cell culture.

2. Materials and methods

2.1. ENM synthesis and preparation

Eight 2D ENMs were generated, extensively characterized, and provided for this study by the Engineered Nanomaterials Coordination Core (ERCC) of the Nanotechnology Health Implications Research (NHIR) Consortium at the Harvard T.H. Chan School of Public Health (Table 1; Table S1). Nanomaterials were produced by liquid-phase exfoliation and/or derivatives of Hummer's Method (Table S2; Parviz et al., 2020) and used as specified for *in vitro* dosimetry (DeLoid et al., 2017).

ENM solutions were prepared in advance of exposure to cells. Aliquots of each nanomaterial liquid suspension were taken from the University of California Davis supply provided by the ERCC, opened within a HEPA-filtered chamber. ENM aliquots were sonicated in a 15-mL conical tube using a calibrated Q500 cup-horn sonicator (QSonica Sonicators; 500 W, 20 kHz, 90% Amp; Newtown, CT), diluted with air-liquid interface cell culture media in a sterile environment to reduce the initial dispersion concentration by 50%, then sonicated again to prevent aggregation. Each 2D ENM sonication was conducted for 15 min total, in intervals of 5-min sonication followed by 30 s of vortexing at high speed, consistent with the NHIR-provided protocol in the nanoparticle characterization reports. Metal oxides used as controls, vanadium pentoxide (V_2O_5) and citrate-capped gold nanoparticles (AuNP), were sonicated according to the protocol for fast-settling nanoparticles by Cohen et al. (2018). Ice was added to the sonicator water as needed to prevent warming of the sonicator water. All diluted nanomaterial suspensions were used for exposure immediately after preparation.

2.2. Animals

Adult male and female C57Bl/6 mice were purchased from Envigo (Envigo Livermore CA; Indianapolis, IN) and were bred to establish a colony. All mice were housed in a particle air-filtered barrier facility consistent with American Association for Accreditation of Laboratory Animal Care approved facilities, on a 12-h light-dark cycle and food and water *ad libitum*. All animal experiments were performed under Institutional Animal Care and Use Committee-approved protocols and according to NIH guidelines.

2.3. Cell culture: mouse tracheal epithelial cells

Primary mouse tracheal epithelial cell (mTEC) cultures were established using a protocol adapted from You and Brody (2013). Adult (8–14 weeks) male C57Bl/6 colony mice

were euthanized with an overdose of pentobarbital (Fatal-Plus, Vortech Pharmaceuticals; Dearborn MI), and each trachea was extracted. Harvested tracheas were then microdissected to remove non-tracheal tissues (esophagus, connective tissue, upper airways) and digested in pronase solution (0.15% *w/v*; Sigma; St. Louis, MO) overnight. To remove non-epithelial cells, the resulting cell suspension was incubated on a Primaria plate (Corning; Corning, NY) for 3–4 h. Remaining mTECs were then collected and plated onto collagen-coated (Rat Tail Collagen I, BD Biosciences; Franklin Lakes, NJ) hanging cell culture inserts (Transwell Costar, Corning; Corning, NY) in a 12-well plate. Plates were seeded from 75,000 to 22,500 cells/well, depending upon the mTEC harvest yield. Cells were incubated at 37 °C, 5.0% CO_2, and 91% relative humidity. Cells were initially cultured on the Transwell membrane with mTEC growth media in both basal and apical wells, with media changes every 48 h or earlier, until confluent; mTEC growth media contained: Dulbecco's Modified Eagle's Medium (DMEM/F12; Gibco; Waltham, MA), 10 μg/mL insulin (Sigma), 5 μg/mL transferrin (Sigma), 0.1 μg/mL cholera toxin (Sigma), 25 ng/mL epidermal growth factor (Corning), 0.03 mg/mL bovine hypothalamus extract (R. Wu et al., 1986), 5% fetal bovine serum (Gibco), and 50 nM retinoic acid (Sigma).

Once confluent, mTECs were cultured at an air-liquid interface (ALI) to induce cell differentiation (You and Brody, 2013). Cultured cells were supplemented with a medium containing DMEM/F12, 5 μg/mL insulin, 5 μg/mL transferrin, 0.025 μg/mL cholera toxin, 5 ng/mL epidermal growth factor, 0.03 mg/mL bovine hypothalamus extract (R. Wu et al., 1986), 1 mg/mL bovine serum albumin (Sigma), and 50 uM retinoic acid. Cells were kept on ALI media between 10 and 21 days to promote cell differentiation (You and Brody, 2013). The medium was added to the basal well only and was replaced approximately every 48 h. Apical wells were washed with 1× sterile PBS during media changes to remove cell waste. Differentiation was confirmed by texture under brightfield microscopy.

2.4. Cell culture: human alveolar epithelial cells

Continuous human alveolar epithelial cells (A549) were purchased from the American Type Culture Collection (ATCC; Manassas, VA). This A549 cell line (CCL-185) was derived from lung carcinoma from a 58-yrold Caucasian male (Giard et al., 1973). The A549 cells were cultured on adherent flasks coated with collagen (Rat Tail Collagen I). The A549 growth media contained: Dulbecco's Modified Eagle's Medium (DMEM/F12), 10% fetal bovine serum, and penicillin/streptomycin at 100 units/mL (Gibco). Media was changed approximately every 48 h. Cells were passaged between three and nine times (compliant with manufacturer's instructions) before seeding on assay plates (2.5×10^5 cells/mL for 12-well plates; $1.0–1.5 \times 10^6$ cells/mL for 96-well plates). Once the A549 cells in assay plates were confluent, they were exposed to nanomaterials.

2.5. Cell culture: human telomerase reverse transcriptase-immortalized corneal epithelial cells

Human telomerase reverse transcriptase-immortalized corneal epithelial (hTCEpi) cells graciously donated by James Jester, PhD (University of California Irvine), were used between passage 36 and 50. The hTCEpi cells were cultured in growth medium composed of EpiLife® (Life Technologies; Carlsbad, CA) supplemented with 1% EpiLife Defined

Growth Supplement (EDGS®; a proprietary combination of bovine serum albumin, bovine transferrin, hydrocortisone, recombinant human-like growth factor type-1, prostaglandin, and recombinant human epidermal growth factor (Life Technologies) and 1% penicillin-streptomycin-amphotericin B (PSF, Lonza; Walkersville, MD).

2.6. Cytotoxicity assay: fluorescent direct cell counting

The cytotoxicity of eight 2D ENMs was tested in primary mTEC culture using differentiable permeability of cell dyes. After 24 h of ENM exposure, permeable (dead) cells were stained with ethidium homodimer-1 (1×10^{-5} M; Molecular Probes, Invitrogen; Waltham, MA), fixed in 1% paraformaldehyde, and all cells were counterstained with 1×10^{-5} M 4′,6-diamidino-2-phenylindole (DAPI; Molecular Probes, Invitrogen). Transwell membranes were then excised from the hanging cell culture inserts and mounted to glass slides using fluorescent mounting medium (Vectashield Antifade Mounting Medium; Vector Laboratories; Burlingame, CA). Slides were stored at 4 °C in darkness until imaged a few days later using a BH2-RFCA microscope (Olympus; Shinjuku, Tokyo, Japan) with a UV filter cube. Ten random images were captured per slide, then extrapolated by area to estimate the total amount of cells. Image files were processed *via* ImageJ (Version 1.5 or later) to calculate percent density, as dead cells would slough off from the Transwell membrane prior to fixation, and normalized to media controls. Following the initial screening of all eight 2D ENMs, several doses of hBN (8, 20, 40, 80 μg/mL) were then used to generate a dose response in mTECs.

The cytotoxicity of hBN was tested in A549 cells using differentiable permeability to fluorescent nuclear dyes. Several doses of hBN (8, 20, 40, 80 μg/mL) were used to generate a dose response. After 24 h of ENM exposure, permeable (dead) cells were stained with 1×10^{-5} M ethidium homodimer-1 (Molecular Probes, Invitrogen) and fixed in 1% paraformaldehyde. All cells were counterstained with 1 uM YO-PRO-1 Iodide (491/509; Molecular Probes, Invitrogen). Plates were stored at 4 °C in darkness before imaging with either a B*Z*-X810 All-in-One Fluorescence microscope (Supplemental Fig. 1; Keyence; Itasca, IL) or confocal microscope (Fig. 4; Leica Microsystems SPE LSI; Buffalo Grove, IL): 488 nm and 561 nm excitation lasers, and using the Z-stack function to capture a 3-dimensional projection of the cells in the well. Eight random images from each well of the 12-well plate were captured, then extrapolated by area to estimate the total amount of cells per well. Image files were processed *via* ImageJ (Version 1.5 or later) to calculate percent density – to remain consistent with measurements from the initial cytotoxicity screening in mTECs – and normalized to media controls.

2.7. Cytotoxicity assay: Calcein AM assay

Calcein AM assay was used to assess the cytotoxicity of hBN and MoS_2 on hTCEpi cells. The hTCEpi cells were plated into 96-well plates at a density of 8000 and 2000 cells per well, respectively, in 100 μL culture medium 24 h prior to treatment to be allowed to attach. Viable hTCEpi cells were fluorescently labeled by Calcein-AM (TREVIGEN®, R&D Systems, Inc.; Minneapolis, MN) following a 24 h incubation with hBN and MoS_2. Citrate-capped AuNPs (5 μg/mL), and an equal volume of deionized water (DW) to the treatment volume of the ENM suspensions were used as negative and vehicle controls, respectively.

Saponin (1 mg/mL; Alfa Aesar; Ward Hill, MA) was used as positive control for loss of cell viability. The fluorescence intensity was measured with a 490 nm excitation filter and a 520 nm emission filter using a microplate spectrophotometer (Synergy 4; BioTek, Instruments Inc.; Winooski, VT). All viability tests were performed in triplicate. The relative cell viability (%), relative to vehicle control wells, was calculated by (absorbance of treated cells - absorbance of blank)/(absorbance of vehicle control - absorbance of blank) × 100.

2.8. Cell migration assay

Inhibition of cellular migration (wound healing) by hBN was evaluated in continuous A549 cell culture using the Oris™ 96-well cell migration assay kit (Platypus Technologies; Fitchburg, WI) per the manufacturer's instructions. The 96-well plate was first coated in collagen (Rat Tail Collagen I), a silicone stopper was inserted into the middle of each well, and then A549 cells were seeded ($1.0–1.5 \times 10^6$ cells/mL) in each well of the 96-well plate, except the outer ring of wells due to concerns with those wells drying out. Once cells were confluent, the silicone stoppers were removed to allow for cellular migration towards the well center, and exposed to hBN *via* cell media. Exposure lasted for either 24-h with hBN present the entire duration, or for the initial 2-h with hBN present and the remaining 22-h with normal growth media for a recovery period. Following exposure, all cells were fixed in 1% paraformaldehyde and stained with 1 uM YO-PRO-1 Iodide (491/ 509; Molecular Probes, Invitrogen). Plates were stored at 4 °C in darkness for a few days before imaging with a confocal microscope (Leica Microsystems SPE LSI), 488 nm excitation laser, and using the Z-stack function to capture a 3-dimension projection of the cells in each well. Each well of the 96-well plate was imaged in entirety.

Cell migration was characterized by the percent closure of the area of detection (pre-migration area - post-migration area/post-migration area) following removal of the rubber stopper from the well. One well per plate row had the stopper removed just prior to fixation, and served as the standard area of the stopper for that row. The negative media control well had the stopper removed at the same time as the treatment wells, and served as an example of cell migration into the void left once the stopper was removed. Vanadium pentoxide (V_2O_5), a nanomaterial known to inhibit cell migration in immortalized human corneal epithelial cells (Kim et al., 2020), was used as a positive control along with cytotoxic hydrogen peroxide. Several doses of hBN (8, 20, 40, 80 μg/mL) were used to generate a dose response.

2.9. Statistical analysis

Statistical analysis was performed with GraphPad Prism v9.1.2 (GraphPad Software Inc.) Data were provided as mean ± standard error of the mean (SEM). Data sets were analyzed by unpaired Student's *t*-test, with Welch's correction for certain analyses. Values where $P < 0.05$ were considered statistically significant.

3. Results

3.1. Select nanomaterials were cytotoxic in primary tracheal cell culture

Eight 2D ENMs were first screened in primary mTECs at a high dose (125–250 μg/mL) derived from the initial nanomaterial solution dispersion concentration. Of the eight nanomaterials tested, reduced graphene oxide (2 um), partially reduced graphene oxide (400 nm), and hBN were cytotoxic to mTECs (Fig. 1).

There was no consistent diameter size among the cytotoxic nanomaterials. The remaining five nanomaterials — graphene 110 nm, graphene oxide 400 nm, graphene oxide 250 nm, reduced graphene oxide 400 nm, and MoS_2 400 nm — were not significantly cytotoxic to mTECs (Fig. 1). The dispersant for six of the nanomaterials, sodium cholate, was not cytotoxic at 1 mg/mL in mTEC culture (Fig. 2).

3.2. hBN showed cytotoxicity in alveolar epithelial cells

Hexagonal boron nitride was cytotoxic to mTECs at 200 μg/mL (Fig. 1); this nanomaterial was chosen to undergo additional cytotoxicity testing due to its small size and ability to deposit deep in the lung (Fig. 3).

A dose response of hBN determined it to be cytotoxic to A549 cells at lower doses of 40 and 80 μg/mL, but was not cytotoxic to mTECs at the same or lower doses (Fig. 4). The 80 μg/mL dose of hBN in A549 cells was very cytotoxic ($P < 0.0001$), decreasing cell viability to approximately 25% of the control group (Fig. 4). Some morphological changes were also seen in the A549 cells at 80 μg/mL (Supplemental Fig. 1). Doses of 8 μg/mL and 20 μg/mL of hBN showed a trend of cytotoxicity towards A549 cells, but this trend was not statistically significant.

3.3. Inhibition of cell migration by hBN

The potential hBN-induced inhibition of cell migration (wound healing) was tested in A549 cells for a continuous 24-h period, or the initial 2 h of a 24-h period. Cellular migration was characterized by the percent closure of the area of detection. Negative values indicated a cytotoxic response, as the cells around the area of detection were ablated. After the 24-h exposure period, hBN significantly inhibited cell migration at 80 μg/mL ($P < 0.001$); there was a trend of inhibition at 40 μg/mL but was not significant (Fig. 5).

However, when cells were only exposed to hBN for 2 h and then allowed to recover for the remaining 22 h, hBN did not significantly inhibit cell migration at any tested dose (Fig. 5). Sub-cytotoxic doses of hBN (8 & 20 μg/mL) also did not significantly inhibit wound healing after the 24-h exposure period (Fig. 5).

3.4. hBN and MoS_2 were cytotoxic to corneal epithelial cells

Hexagonal boron nitride and MoS_2 were tested for corneal cytotoxicity in hTCEpi cells; hBN significantly decreased cell viability in hTCEpi cells at four tested doses (4, 10, 20, & 40 μg/mL), but not at the lowest tested doses of 0.04, 0.4, and 2 μg/mL (Fig. 6). Cell

viability of hTCEpi cells was also significantly decreased by MoS_2 (2.5, 5,12.5, 25, & 50 μg/mL), while 0.05 and 0.5 μg/mL had no significant effect (Fig. 6).

4. Discussion

In this study, we tested multiple 2D ENMs for *in vitro* toxicity in pulmonary and corneal epithelial cells. Eight 2D ENMs were initially tested in primary mTEC cultures; partially reduced graphene oxide (400 nm), reduced graphene oxide (2 um), and hBN (150 nm) were found to be cytotoxic (Fig. 1). Mouse tracheal epithelial cell culture was chosen for the initial screening due to our desire for a mixed cell population and consideration towards mucociliary clearance. The mouse upper trachea is comprised of pseudostratified epithelium with glands, which more closely resembles the mixed cell-type epithelium of the trachea and bronchi in humans. The epithelium of the lower trachea in the mouse is pseudostratified without glands, similar to human bronchioles greater than 1 mm in diameter. This range of epithelial cell types allowed us to model a larger region of the lung as relevant to humans. In the case of an *in vivo* exposure, the trachea epithelium would be exposed to any nanomaterials as they are removed *via* mucociliary clearance.

There were challenges associated with creating a reliable measure of toxicity in primary cell culture. Primary mTECs have high enzymatic activity, and thus cytotoxicity could not be measured using assay kits reliant on enzymes, such as luciferase-or esterase-based assays. To circumvent this challenge, we developed a system for direct cell counting using fluorescent dyes with differentiable permeability; dead cells were distinguished from other cells by dye color. Primary mTECs were grown using air-liquid interface to permit cellular differentiation, but dead cells also had a tendency to slough off of the Transwell membrane prior to fixation. Thus, we used percent cell density as our endpoint measure to account for dead cells no longer on the membrane. Direct cell counting was standardized through a thresholding workflow in ImageJ to decrease human error and improve throughput capacity, allowing us to test several different nanomaterials.

The biosurfactant sodium cholate was used as the dispersion solution for multiple ENMs, acting as a stabilizer for nanoparticles suspended in solution. At 1 mg/mL, sodium cholate was not cytotoxic to mTECs (Fig. 2). Additionally, the nanomaterial graphene (110 nm) contained the highest dose of sodium cholate (2.5 mg/kg) in exposure, but was not cytotoxic to mTECs (Fig. 1). Other cytotoxic nanomaterials had lower doses of sodium cholate in comparison, thus sodium cholate is not thought to drive cytotoxicity.

Hexagonal boron nitride (hBN) was selected for further testing due to its initial cytotoxicity in mTECs and small diameter of 150 nm. A dose response of hBN in mTECs yielded no significant cytotoxicity at the tested doses (8–80 μg/mL; Fig. 4). The diameter of hBN, 150 nm, is a particle size capable of deposition deep in the lung (Fig. 3). Size-dependent deposition of nanomaterials and other particles in the lung has been widely observed (Braakhuis et al., 2014; Carvalho et al., 2011). Particles with the greatest level of alveolar deposition range in size from 10 and 100 nm, however, the Multiple-Path Particle Dosimetry model demonstrates alveolar deposition continues to occur at 150 nm and beyond (Löndahl et al., 2014). A particle size of 300 nm appears to be the upper limit for alveolar deposition

(Löndahl et al., 2014; Newman and Chan, 2008). Thus, we consider it likely that hBN (150 nm) could deposit in the alveolar region and was of interest for further cytotoxicity testing.

Human alveolar epithelial cells (A549) were utilized to test hBN cytotoxicity in the more distal airway. A549 cells were chosen over other lung epithelial cell culture models, such as normal human bronchial epithelial cells (BEAS-2B), for a few select reasons. A549 cells are often used as a model for alveolar type II cells, which was more representative of the expected deposition site of hexagonal boron nitride than the cuboidal cells found in bronchial epithelium. A549 cells also grow as a confluent monolayer, whereas BEAS-2B cells grow as a multilayer (Schlinkert et al., 2015). A monolayer was required for the Oris™ 96-well cell migration assay, stated in the manufacturers' instructions (Methods 2.8). A cell monolayer also receives a homogenous concentration of culture media (Tibbitt and Anseth, 2009); since the nanomaterial exposure occurred through the media, this was a means to keep the dose of nanomaterials that cells were exposed to more consistent. Another concern of BEAS-2B cell culture was the known sensitivity to culture conditions and resulting phenotypic changes that alter measurements of metal toxicity (Zhao and Klimecki, 2015). While not generalizable, it is noteworthy that cytotoxicity following exposure to the nanomaterial titanium dioxide (TiO2) was reported to be similar between both A549 cells and BEAS-2B cells (Biola-Clier et al., 2016).

A dose response of hBN demonstrated a cytotoxic response in A549 cells at doses as low as 40 μg/mL (Fig. 4), in contrast to expected results, as this is an immortalized cell line which was expected to be more robust in the face of cytotoxicity. Mittal et al. (2016) has shown through transmission electron microscopy that multiple graphene-based 2D nanomaterials are internalized by A549 cells; nanomaterial internalization increased with dose, but varied by nanomaterial and by cell type, with A549 cells having increased ENM internalization compared to immortalized human bronchial epithelial (BEAS-2B) cells. Hexagonal boron nitride has been shown to enter human umbilical vein endothelial cells (cell size: ~17 um) and human dermal fibroblasts (şen et al., 2019), and thus we hypothesize hBN has decent internalization into similarlysized A549 cells (cell size: ~15 um). In this study, we hypothesize that the presence of ciliated cells and mucus secreted by mucus cells of the epithelium — both found in primary mTEC cultures but not A549 cultures — improve clearance, decrease uptake, and reduce toxicity of hBN.

The use of A549 cells also allowed us to test inhibition of wound healing by hBN in a cellular migration assay, in which a robust cell line is required for successful assay completion. Hexagonal boron nitride was not found to significantly inhibit A549 wound healing at 8, 20, or 40 μg/mL (Fig. 5), but was again cytotoxic to A549 cells at 80 μg/mL. In contrast, a previous study (şen et al., 2019) found that hBN stimulated wound healing in human umbilical vein endothelial cells (HUVECs; 25 μg/mL) and human dermal fibroblasts (HDFs; 25, 100, 200 μg/mL) after 24 h, using scratch assay. Uptake of hBN into both cell types was observed at the tested doses (şen et al., 2019). We utilized a stopperbased assay that was previously shown to be successful for measuring nanomaterial inhibition of wound healing in ocular epithelial cells (Kim et al., 2020). Interestingly, şen et al. (2019) also found hBN increased cell viability in HUVECs at lower doses (10–100 μg/mL) — a dose within the range for cytotoxicity in A549 cells (Fig. 4) — but hBN was still cytotoxic at

higher doses (300–500 μg/mL for HUVECs, 150–500 μg/mL for HDFs). Study differences include cell type as well as particle size (50–70 nm hBN *vs.* our 150 nm hBN), could both contribute to differing results. Hexagonal boron nitride may be more advantageous in certain cell types, but have more adverse effects in others, and thus cell typespecific testing should be performed prior to the use of hBN in any consumer or biomedical application.

In addition to the lung, the eye is also an important exposure site for aerosolized nanomaterials. Both airway and corneal epithelia interface with the external environment; the continuous cell layer provides the first barrier against injury by xenobiotics. Epithelial cells are tightly joined to others in a continuous sheet to maintain an effective barrier. Injury and cell death among epithelial cells can comprise defensive barriers and allow xenobiotics to enter deeper towards crucial tissues. Both the lung and the eye are organ systems in which damage to the epithelial cell layer could have detrimental impacts to underlying essential tissues. We tested the non-graphene 2D nanomaterials — hBN and MoS_2 — for cytotoxicity in an immortalized human corneal epithelial cell line. Both nanomaterials were cytotoxic to hTCEpi cells, with hBN cytotoxic from 4 to 40 μg/mL and MoS_2 cytotoxic from 2.5 to 50 μg/mL. Hexagonal boron nitride was also cytotoxic to lung epithelial cells, albeit at higher doses (Fig. 4), while MoS_2 was not cytotoxic to primary mTEC culture. Increased sensitivity to cytotoxicity by nanomaterials may be attributed to differences in the epithelial cell types - such as the production of protective mucus or surfactant by lung epithelium. The lack of cytotoxicity by MoS_2 in primary mTECs may be due to robust mucus secretion of differentiated airway cells permitted by primary cell culture, which would not have been possible in immortalized cell lines nor corneal epithelial cells which lacks secretory cells. The area of surface exposure and cell types are important considerations in the evaluation of occupational exposure limits, as one aerosolized nanomaterial may affect first-contact tissue sites in an asymmetrical manner.

The scope and scale of this study prohibited us from testing the two graphene-based nanomaterials cytotoxic potential further in primary murine tracheal epithelial cell culture, although further examination is certainly warranted. Reduced graphene oxide and partially reduced graphene oxide contain residual oxygen atoms, which have the potential to create oxidative stress that results in cytotoxicity (Fu et al., 2014; Mittal et al., 2016). ROS generation is also the same mechanism that provides graphene oxide with its antimicrobial properties (S. Liu et al., 2011) or chemotherapeutic potential (Tabish et al., 2018). Reduced graphene oxide, when compared to graphene oxide, had increased oxidative stress and macrophage inflammation (Y. Wu et al., 2018).

It is important to note that dose, size, and nanoparticle surface area (Gatoo et al., 2014) are all factors that can influence the toxicity of nanomaterials. The uniquely-high surface area of 2D ENMs creates a phenomenon where ENM effect is not proportional to mass, and thus smaller nanomaterials could have more devastating effects on biological systems. Ma et al. (2015) have shown that graphene oxide nanoparticles with a smaller lateral size have increased cellular uptake, and there is a size-dependent interaction between graphene oxide nanoparticles and the plasma membrane. Greater levels of graphene oxide-membrane interaction results in cell membrane gene dysregulation and increased macrophage cell

damage (Xu et al., 2016). A similar mechanism may mediate graphene oxide toxicity on epithelial cells.

Non-cytotoxic ENMs are excellent materials-of-interest for use in consumer and medical products. In our findings, other graphene-based nanomaterials (graphene 110 nm, graphene oxide 250 nm and 400 nm, and reduced graphene oxide 400 nm), as well as MoS2 (400 nm), were not cytotoxic in primary mTEC culture (Fig. 1). The lack of cytotoxicity in a mixed cell-type respiratory epithelial model warrants further investigation for possible therapeutic use in respiratory applications; there are several studies applying nanoparticles in the treatment of lung diseases like cancer and asthma (Kenyon et al., 2013; Lu et al., 2014; Roa et al., 2011).

Quality control and consistent synthesis of nanomaterials is also an important consideration when investigating toxicity or therapeutic potential of nanomaterials. This is an advantage of this study, in that the tested nanomaterials were produced by the Engineered Nanomaterials Coordination Core (ERCC) of the Nanotechnology Health Implications Research (NHIR) Consortium at the Harvard T. H. Chan School of Public Health, with detailed characterization reports supplied for each nanomaterial (available in supplement).

5. Conclusions

Our study demonstrates hexagonal boron nitride (hBN) was cytotoxic at a high dose in primary mouse tracheal epithelial cells (200 μg/mL), cytotoxic at moderate doses to immortalized human alveolar epithelial cells (40/80 μg/mL), and cytotoxic at lower doses to human corneal epithelial cells (4/10/20/40 μg/mL). Wound healing was not inhibited at any sub-cytotoxic hBN dose in immortalized human alveolar epithelial cells. Further directions should examine the *in vivo* effects of aerosol exposure to hBN. Based on cell/tissue type and anatomical site, particle clearance and repair mechanisms might affect nanomaterial toxicity.

Supplementary Material

Refer to Web version on PubMed Central for supplementary material.

Acknowledgements

This publication was supported by the National Institute of Environmental Health Sciences of the National Institutes of Health (NIEHS U01ES027288) as part of the Nanotechnology Health Implications Research (NHIR) Consortium. The content is solely the responsibility of the authors and does not necessarily represent the official views of the National Institutes of Health. Engineered nanomaterials used for this publication have been synthesized, characterized, and provided by the Engineered Nanomaterials Resource and Coordination Core established at the Harvard T. H. Chan School of Public Health (NIH U24ES026946) as part of the Nanotechnology Health Implications Research Consortium. The authors would like to thank Philip Demokritou, Dimitrios Bitounis, and the rest of the Nanosafety Research Center for their roles in providing the nanomaterials, as well as Dale Uyeminami for maintenance of the UC Davis nanomaterial supply. Graphical abstract was created with BioRender.com. Confocal (NIH S10RR026422) and brightfield fluorescent imaging were conducted using the Cellular and Molecular Imaging Core Facility at UC Davis Center for Health. Morgan Domanico's effort was supported by the UC Davis Lung Center Training in Comparative Lung Biology and Medicine Program (T32 HL007013) and J-M Bustamante's effort by the UC Davis Advanced Training in Environmental Health Sciences Program (T32 ES007059). Sara Thomasy is supported by NEI R01 EY09970. We acknowledge core support from the UC Davis Environmental Health Sciences Center P30 ES023513.

References

Arvidsson R, Molander S, Sandén BA, 2013. Review of potential environmental and health risks of the nanomaterial graphene. Hum. Ecol. Risk Assess. Int. J 19 (4), 873–887. 10.1080/10807039.2012.702039.

Balandin AA, 2011. Thermal properties of graphene and nanostructured carbon materials. Nat. Mater 10 (8), 569–581. 10.1038/nmat3064. [PubMed: 21778997]

Biola-Clier M, Beal D, Caillat S, Libert S, Armand L, Herlin-Boime N, Carriere M, 2016. Comparison of the DNA damage response in BEAS-2B and A549 cells exposed to titanium dioxide nanoparticles. Mutagenesis 32 (1), 161–172. 10.1093/mutage/gew055. [PubMed: 27803034]

Braakhuis HM, Gosens I, Krystek P, Boere JA, Cassee FR, Fokkens PH, Park MV, 2014. Particle size dependent deposition and pulmonary inflammation after short-term inhalation of silver nanoparticles. Part. Fibre Toxicol 11, 49. 10.1186/s12989-014-0049-1. [PubMed: 25227272]

Carvalho TC, Peters JI, Williams RO, 2011. Influence of particle size on regional lung deposition – what evidence is there? Int. J. Pharm 406 (1), 1–10. 10.1016/j.ijpharm.2010.12.040. [PubMed: 21232585]

Chang C-J, Yang H-H, 2020. Impact on eye health regarding gaseous and particulate pollutants. Aerosol Air Qual. Res 20 (7), 1695–1699. 10.4209/aaqr.2020.03.0098.

Chen S, Moore AL, Cai W, Suk JW, An J, Mishra C, Ruoff RS, 2011. Raman measurements of thermal transport in suspended monolayer graphene of variable sizes in vacuum and gaseous environments. ACS Nano 5 (1), 321–328. 10.1021/nnl02915x. [PubMed: 21162551]

Chen S, Wu Q, Mishra C, Kang J, Zhang H, Cho K, Ruoff RS, 2012. Thermal conductivity of isotopically modified graphene. Nat. Mater 11 (3), 203–207. 10.1038/nmat3207. [PubMed: 22231598]

Chilkoor G, Karanam SP, Star S, Shrestha N, Sani RK, Upadhyayula VKK, Gadhamshetty V, 2018. Hexagonal boron nitride: the thinnest insulating barrier to microbial corrosion. ACS Nano 12 (3), 2242–2252. 10.1021/acsnano.7b06211. [PubMed: 29432687]

Cohen JM, Beltran-Huarac J, Pyrgiotakis G, Demokritou P, 2018. Effective delivery of sonication energy to fast settling and agglomerating nanomaterial suspensions for cellular studies: implications for stability, particle kinetics, dosimetry and toxicity. NanoImpact 10, 81–86. 10.1016/j.impact.2017.12.002. [PubMed: 29479575]

DeLoid GM, Cohen JM, Pyrgiotakis G, Demokritou P, 2017. Preparation, characterization, and in vitro dosimetry of dispersed, engineered nanomaterials. Nat. Protoc 12 (2), 355–371. 10.1038/nprot.2016.172. [PubMed: 28102836]

Fiume MM, Bergfeld WF, Belsito DV, Hill RA, Klaassen CD, Liebler DC, Andersen FA, 2015. Safety assessment of boron nitride as used in cosmetics. Int. J. Toxicol 34 (3 Suppl), 53s–60s. 10.1177/1091581815617793. [PubMed: 26684796]

Fu PP, Xia Q, Hwang H-M, Ray PC, Yu H, 2014. Mechanisms of nanotoxicity: generation of reactive oxygen species. J. Food Drug Anal 22 (1), 64–75. 10.1016/j.jfda.2014.01.005. [PubMed: 24673904]

Gatoo MA, Naseem S, Arfat MY, Dar AM, Qasim K, Zubair S, 2014. Physicochemical properties of nanomaterials: implication in associated toxic manifestations. Biomed. Res. Int 2014, 498420 10.1155/2014/498420. [PubMed: 25165707]

Giard DJ, Aaronson SA, Todaro GJ, Arnstein P, Kersey JH, Dosik H, Parks WP, 1973. In vitro cultivation of human tumors: establishment of cell lines derived from a series of solid tumors. J. Natl. Cancer Inst 51 (5), 1417–1423. 10.1093/jnci/51.5.1417. [PubMed: 4357758]

Hoet PH, Brüske-Hohlfeld I, Salata OV, 2004. Nanoparticles – known and unknown health risks. J. Nanobiotechnol 2 (1), 12. 10.1186/1477-3155-2-12.

Hu T, Mei X, Wang Y, Weng X, Liang R, Wei M, 2019. Two-dimensional nano materials: fascinating materials in biomedical field. Sci. Bull 64 (22), 1707–1727. 10.1016/j.scib.2019.09.021.

Jiang X-F, Weng Q, Wang X-B, Li X, Zhang J, Golberg D, Bando Y, 2015. Recent progress on fabrications and applications of boron nitride nanomaterials: a review. J. Mater. Sci. Technol 31 (6), 589–598. 10.1016/j.jmst.2014.12.008.

Kenyon NJ, Bratt JM, Lee J, Luo J, Franzi LM, Zeki AA, Lam KS, 2013. Selfassembling nanoparticles containing dexamethasone as a novel therapy in allergic airways inflammation. PLoS One 8 (10), e77730. 10.1371/journal.pone.0077730. [PubMed: 24204939]

Kim S, Gates B, Leonard BC, Gragg M, Pinkerton KE, Winkle LV, Thomasy SM, 2020. Engineered metal oxide nanomaterials inhibit corneal epithelial wound healing in vitro and in vivo. NanoImpact 17. 10.1016/j.impact.2019.100198.

Lee C, Wei X, Kysar JW, Hone J, 2008. Measurement of the elastic properties and intrinsic strength of monolayer graphene. Science 321 (5887), 385–388. 10.1126/science.1157996. [PubMed: 18635798]

Li J. J.e, Muralikrishnan S, Ng C-T, Yung L-YL, Bay B-H, 2010. Nanoparticle-induced pulmonary toxicity. Exp. Biol. Med 235 (9), 1025–1033. 10.1258/ebm.2010.010021.

Li LH, Cervenka J, Watanabe K, Taniguchi T, Chen Y, 2014. Strong oxidation resistance of atomically thin boron nitride nanosheets. ACS Nano 8 (2), 1457–1462. 10.1021/nn500059s. [PubMed: 24400990]

Liu S, Zeng TH, Hofmann M, Burcombe E, Wei J, Jiang R, Chen Y, 2011. Antibacterial activity of graphite, graphite oxide, graphene oxide, and reduced graphene oxide: membrane and oxidative stress. ACS Nano 5 (9), 6971–6980. 10.1021/nn202451x. [PubMed: 21851105]

Liu Z, Gong Y, Zhou W, Ma L, Yu J, Idrobo JC, Ajayan PM, 2013. Ultrathin high-temperature oxidation-resistant coatings of hexagonal boron nitride. Nat. Commun 4 (1), 2541. 10.1038/ncomms3541. [PubMed: 24092019]

Löndahl J, Möller W, Pagels JH, Kreyling WG, Swietlicki E, Schmid O, 2014. Measurement techniques for respiratory tract deposition of airborne nanoparticles: a critical review. J. Aerosol Med. Pulmon. Drug Deliv 27 (4), 229–254. 10.1089/jamp.2013.1044.

Lu X, Zhu T, Chen C, Liu Y, 2014. Right or left: the role of nanoparticles in pulmonary diseases. Int. J. Mol. Sci 15 (10), 17577–17600. 10.3390/ijms151017577. [PubMed: 25268624]

Lui CH, Liu L, Mak KF, Flynn GW, Heinz TF, 2009. Ultraflat graphene. Nature 462 (7271), 339–341. 10.1038/nature08569. [PubMed: 19924211]

Ma J, Liu R, Wang X, Liu Q, Chen Y, Valle RP, Liu S, 2015. Crucial role of lateral size for graphene oxide in activating macrophages and stimulating pro-inflammatory responses in cells and animals. ACS Nano 9 (10), 10498–10515. 10.1021/acsnano.5b04751. [PubMed: 26389709]

Merlo A, Mokkapati VRSS, Pandit S, Mijakovic I, 2018. Boron nitride nano materials: biocompatibility and bio-applications. Biomater. Sci 6 (9), 2298–2311. 10.1039/C8BM00516H. [PubMed: 30059084]

Mittal S, Kumar V, Dhiman N, Chauhan LK, Pasricha R, Pandey AK, 2016. Physicochemical properties based differential toxicity of graphene oxide/reduced graphene oxide in human lung cells mediated through oxidative stress. Sci. Rep 6, 39548. 10.1038/srep39548. [PubMed: 28000740]

Nardekar SS, Krishnamoorthy K, Pazhamalai P, Sahoo S, Mariappan VK, Kim SJ, 2020. Exceptional interfacial electrochemistry of few-layered 2D MoS2 quantum sheets for high performance flexible solid-state supercapacitors. J. Mater. Chem. A 8 (26), 13121–13131. 10.1039/D0TA01156H.

Nath NCD, Debnath T, Nurunnabi M, Kim E-K, 2019. In vitro toxicity of 2D materials. In: Biomedical Applications of Graphene and 2D Nanomaterials, pp. 165–186.

Newman SP, Chan H-K, 2008. In vitro/in vivo comparisons in pulmonary drug delivery. J. Aerosol Med. Pulmon. Drug Deliv 21 (1), 77–84. 10.1089/jamp.2007.0643.

Oberdörster G, Oberdörster E, Oberdörster J, 2005. Nanotoxicology: an emerging discipline evolving from studies of ultrafine particles. Environ. Health Perspect 113 (7), 823–839. 10.1289/ehp.7339. [PubMed: 16002369]

Parlak O, Tiwari A, Turner APF, Tiwari A, 2013. Template-directed hierarchical self-assembly of graphene based hybrid structure for electrochemical biosensing. Biosens. Bioelectron 49, 53–62. 10.1016/j.bios.2013.04.004. [PubMed: 23708818]

Parviz D, Bitounis D, Demokritou P, Strano M, 2020. Engineering two-dimensional nanomaterials to enable structure-activity relationship studies in nanosafety research. NanoImpact 18, 100226. 10.1016/j.impact.2020.100226. [PubMed: 32617436]

Roa WH, Azarmi S, Al-Hallak MHDK, Finlay WH, Magliocco AM, Löbenberg R, 2011. Inhalable nanoparticles, a non-invasive approach to treat lung cancer in a mouse model. J. Control. Release 150 (1), 49–55. 10.1016/j.jconrel.2010.10.035. [PubMed: 21059378]

Sargent LM, Porter DW, Staska LM, Hubbs AF, Lowry DT, Battelli L, Reynolds SH, 2014. Promotion of lung adenocarcinoma following inhalation exposure to multi-walled carbon nanotubes. Part. Fibre Toxicol 11, 3. 10.1186/1743-8977-11-3. [PubMed: 24405760]

Schlinkert P, Casals E, Boyles M, Tischler U, Hornig E, Tran N, Duschl A, 2015. The oxidative potential of differently charged silver and gold nanoparticles on three human lung epithelial cell types. J. Nanobiotechnol 13 (1), 1. 10.1186/s12951-014-0062-4.

Şen Ö, Emanet M, Çulha M, 2019. Stimulatory effect of hexagonal boron nitrides in wound healing. ACS Appl. Bio Mater 2 (12), 5582–5596. 10.1021/acsabm.9b00669.

Tabish TA, Zhang S, Winyard PG, 2018. Developing the next generation of graphene-based platforms for cancer therapeutics: the potential role of reactive oxygen species. Redox Biol. 15, 34–40. 10.1016/j.redox.2017.11.018. [PubMed: 29197802]

Tibbitt MW, Anseth KS, 2009. Hydrogels as extracellular matrix mimics for 3D cell culture. Biotechnol. Bioeng 103 (4), 655–663. 10.1002/bit.22361. [PubMed: 19472329]

Vance ME, Kuiken T, Vejerano EP, McGinnis SP, Hochella MF Jr., Rejeski D, Hull MS, 2015. Nanotechnology in the real world: redeveloping the nanomaterial consumer products inventory. Beilstein J. Nanotechnol 6, 1769–1780. 10.3762/bjnano.6.181. [PubMed: 26425429]

Wu R, Sato GH, Whitcutt MJ, 1986. Developing differentiated epithelial cell cultures: airway epithelial cells. Fundam. Appl. Toxicol 6 (4), 580–590. 10.1016/0272-0590(86)90170-3. [PubMed: 3519341]

Wu Y, Wang F, Wang S, Ma J, Xu M, Gao M, Liu S, 2018. Reduction of graphene oxide alters its cyto-compatibility towards primary and immortalized macrophages. Nanoscale 10 (30), 14637–14650. 10.1039/C8NR02798F. [PubMed: 30028471]

Xu M, Zhu J, Wang F, Xiong Y, Wu Y, Wang Q, Liu S, 2016. Improved in vitro and in vivo biocompatibility of graphene oxide through surface modification: poly (acrylic acid)-functionalization is superior to PEGylation. ACS Nano 10 (3), 3267–3281. 10.1021/acsnano.6b00539. [PubMed: 26855010]

Yah CS, Simate GS, Iyuke SE, 2012. Nanoparticles toxicity and their routes of exposures. Pak. J. Pharm. Sci 25 (2), 477–491.

You Y, Brody SL, 2013. Culture and differentiation of mouse tracheal epithelial cells. Methods Mol. Biol 945, 123–143. 10.1007/978-1-62703-125-7_9. [PubMed: 23097105]

Zhang Q, Wu Z, Li N, Pu Y, Wang B, Zhang T, Tao J, 2017. Advanced review of graphene-based nanomaterials in drug delivery systems: synthesis, modification, toxicity and application. Mater. Sci. Eng. C Mater. Biol. Appl 77, 1363–1375. 10.1016/j.msec.2017.03.196. [PubMed: 28532014]

Zhao F, Klimecki WT, 2015. Culture conditions profoundly impact phenotype in BEAS-2B, a human pulmonary epithelial model. J. Appl. Toxicol 35 (8), 945–951. 10.1002/jat.3094. [PubMed: 25524072]

Web references

???Jain Prakhar & Prasad Eswara. (2021, July). Nanotechnology in Energy Market - 2030. Allied Market Research. URL: https://www.alliedmarketresearch.com/nanotechnology-in-energy-market.

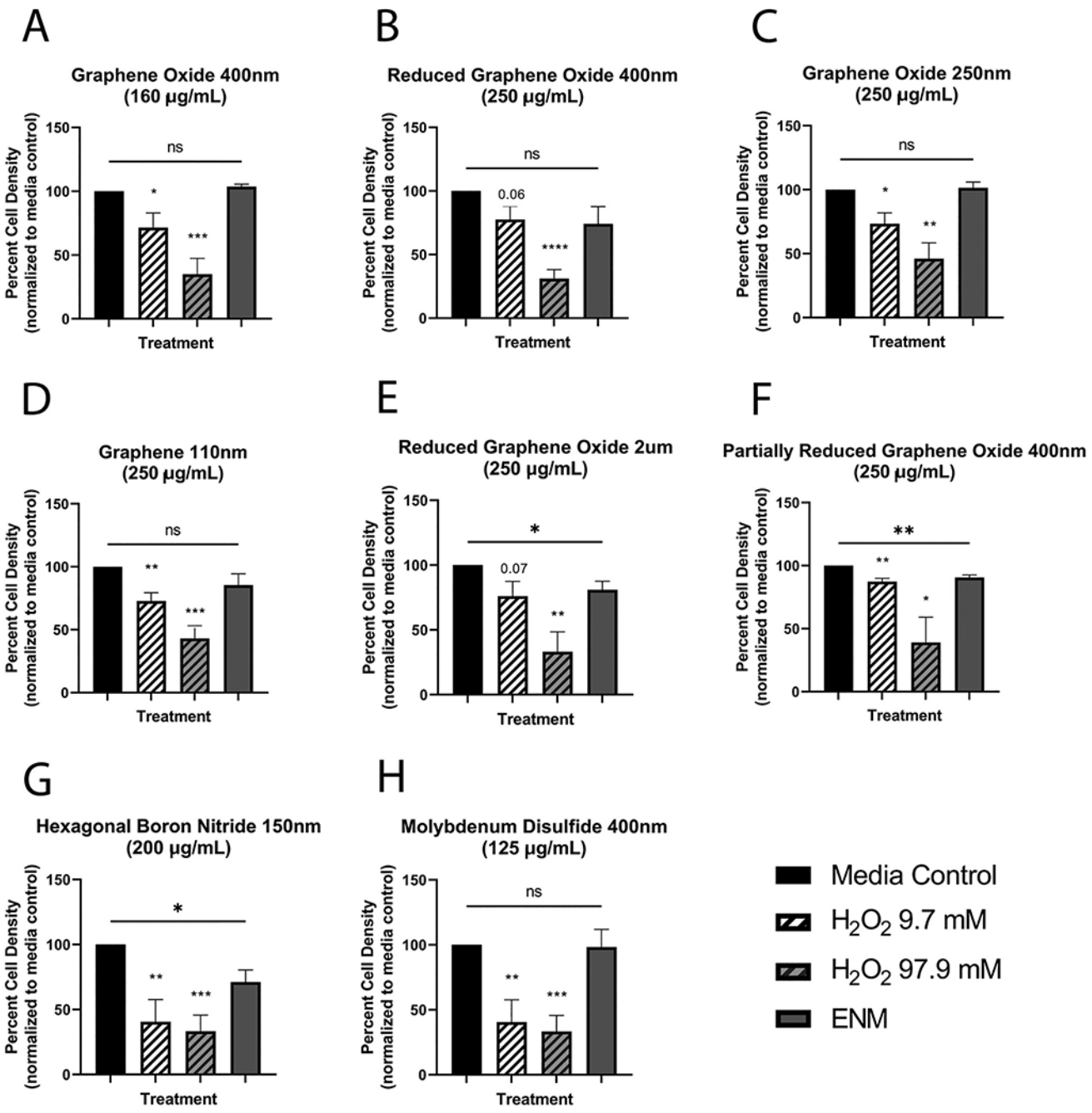

Fig. 1.

Cytotoxicity of eight 2D engineered nanomaterials (ENMs) in primary mouse tracheal epithelial cell culture as percent cell density. Nanomaterials tested included graphene oxide of two sizes (A & C), reduced graphene oxide of two sizes (B & E), graphene (D), partially reduced graphene oxide (F), hexagonal boron nitride (G), and molybdenum disulfide (H). All density values were normalized to the media control of the respective plate. Cytotoxicity was induced in three ENMs: reduced graphene oxide 2 um (250 µg/mL), partially reduced graphene oxide 400 um (250 µg/mL), and hexagonal boron nitride (200 µg/mL). Hydrogen

peroxide (H_2O_2) was used as a positive control for cytotoxicity. An unpaired student's *t*-test was performed to compare each treated group to the media control group: $*P < 0.05$, $**P < 0.01$. $N = 3$ (F), $N = 4$ (C, E), or $N = 5$ (A, B, D, G, H) for all treatment groups.

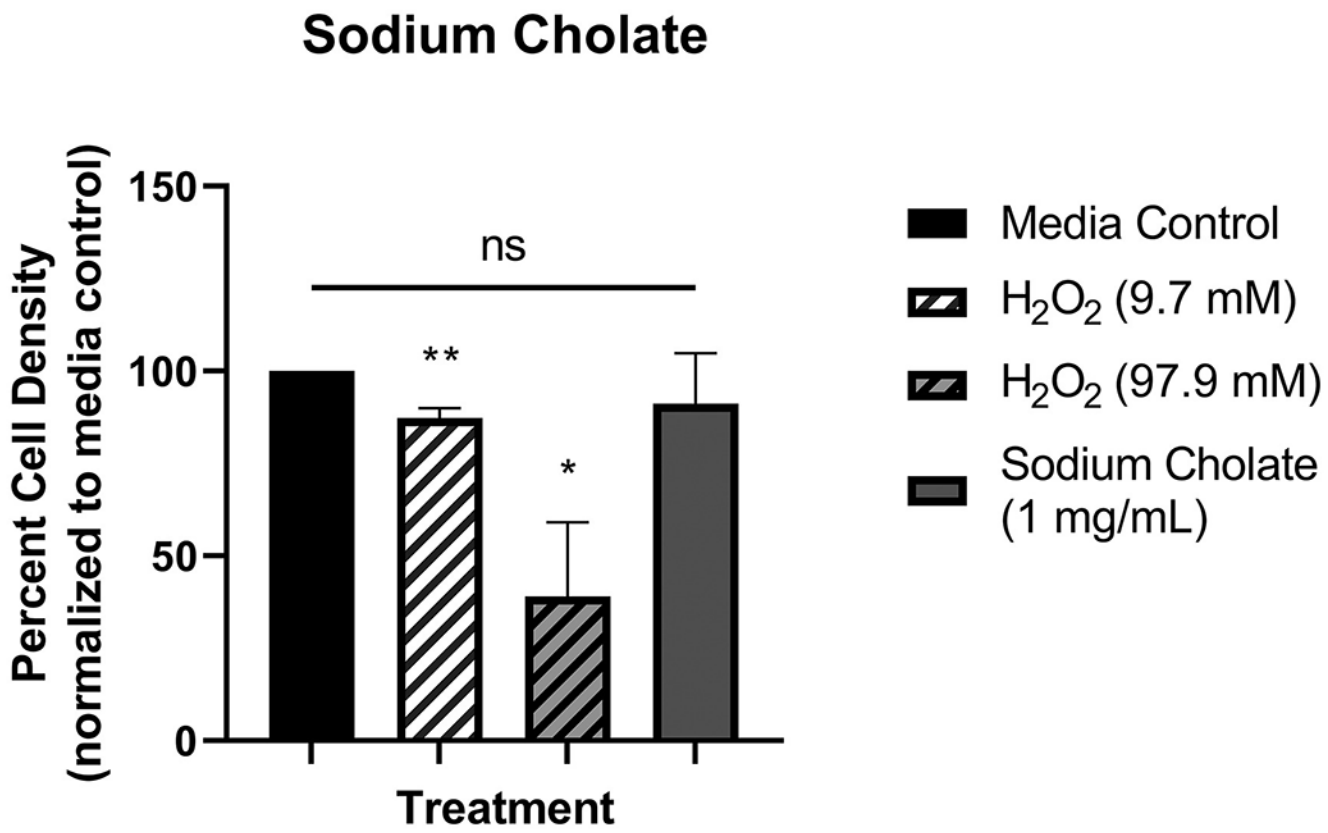

Fig. 2.

Sodium cholate, the dispersant for six of the engineered nanomaterials (ENMs), was tested for cytotoxicity (percent cell density) in primary mouse tracheal epithelial cell culture at 1 mg/kg (A). Comparable sodium cholate concentrations of tested nanomaterials are also provided (B). All density values were normalized to the media control of the respective plate. Hydrogen peroxide (H_2O_2) was used as a positive control for cytotoxicity. An unpaired student's t-test was performed to compare each treated group to the media control group: $*P < 0.05$, $**P < 0.01$. N = 3 for all conditions.

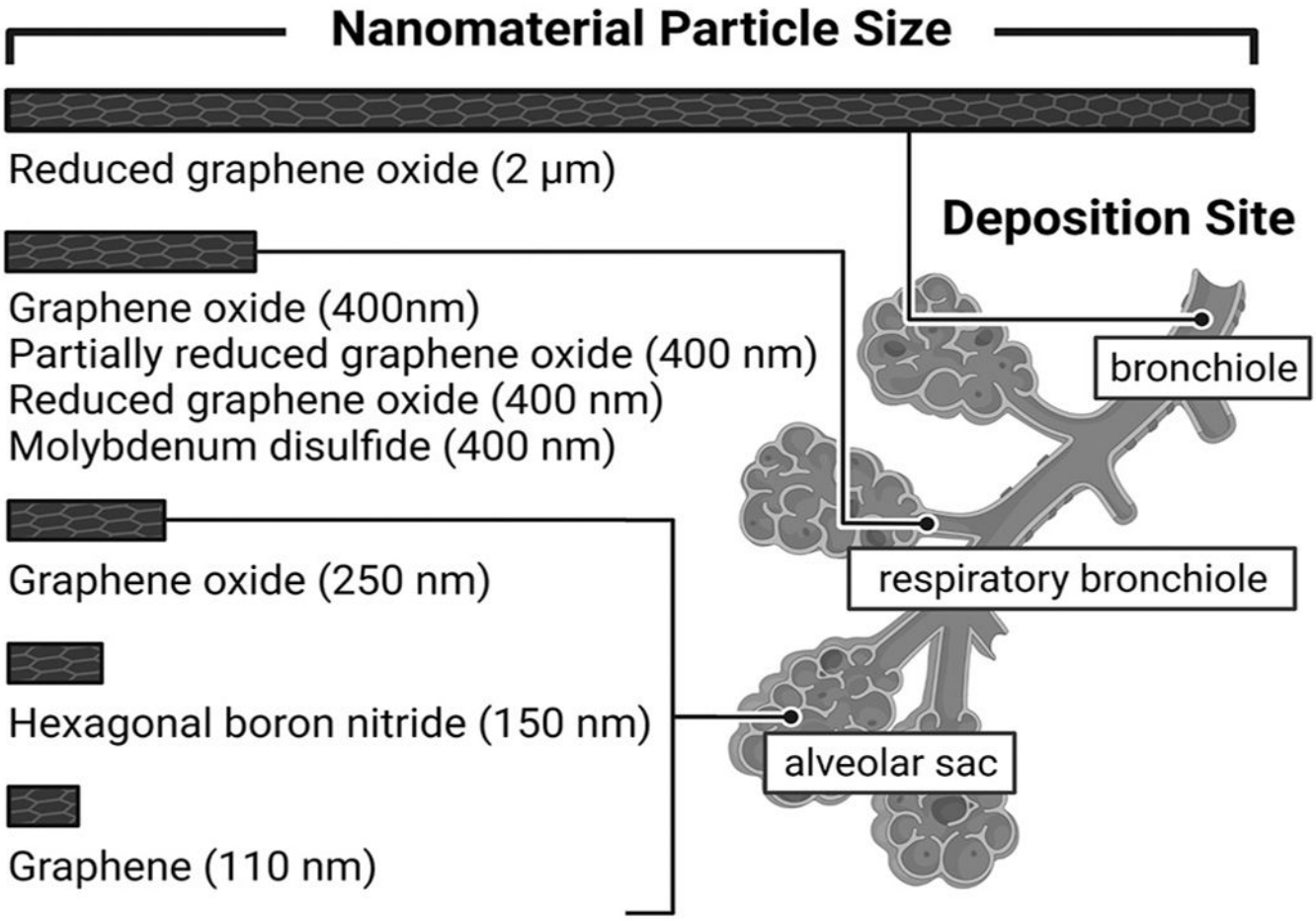

Fig. 3.

A diagram depicting the sizes of the nanomaterials used, and where in the lung these particles would be capable of depositing based on size. Created with BioRender.com.

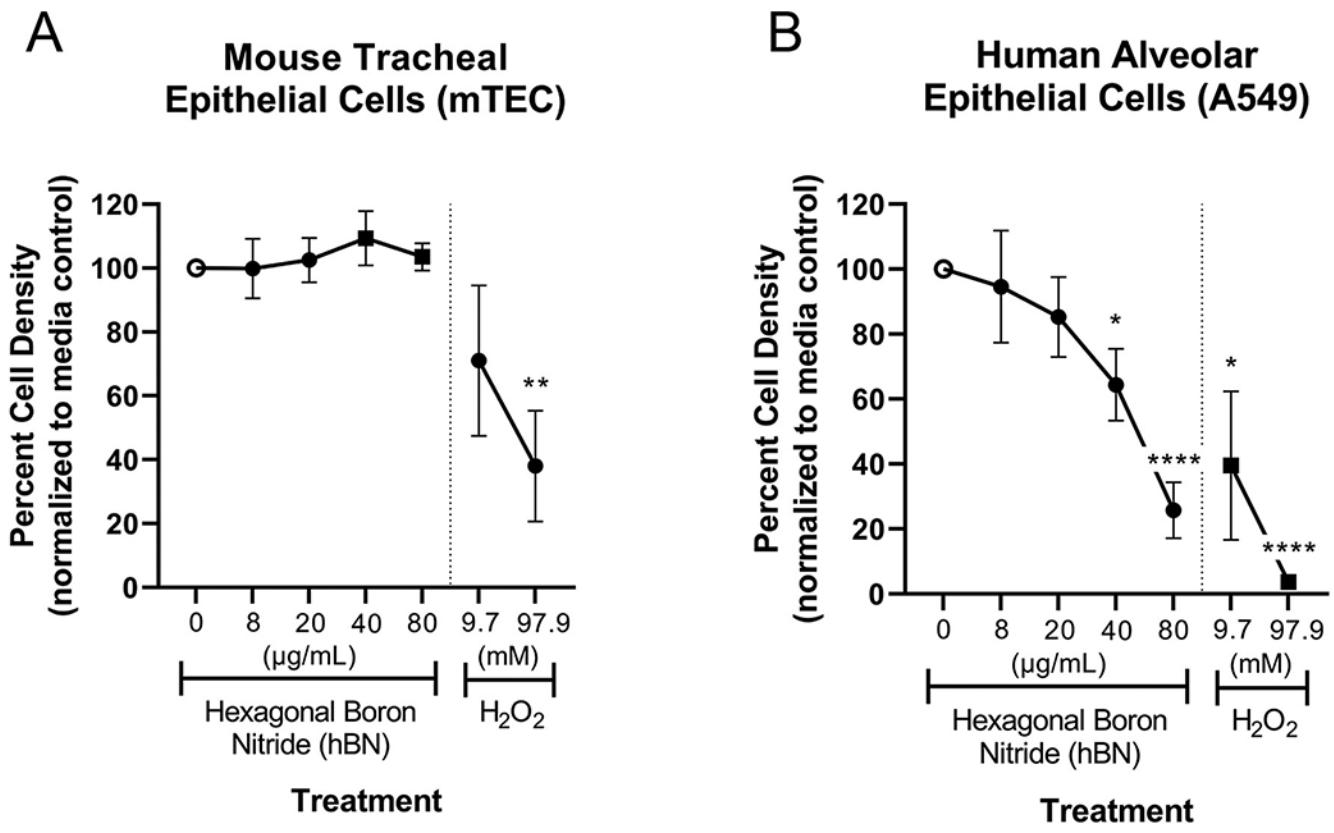

Fig. 4.

Cytotoxicity, measured as percent cell density, following a dose response of hexagonal boron nitride (hBN) in (A) primary mouse tracheal epithelial cell culture (mTEC) and (B) human alveolar epithelial cell culture (A549). All density values were normalized to the media control (0 mg/kg hBN) of the respective plate. Cytotoxicity was induced in A549 cells at 40 µg/mL and 80 µg/mL of hBN. Hydrogen peroxide (H_2O_2) was used as a positive control for cytotoxicity. An unpaired student's t-test was performed to compare each treated group to the media control group: $*P < 0.05$, $**P < 0.01$, $****p < 0.0001$. N = 5 for all groups.

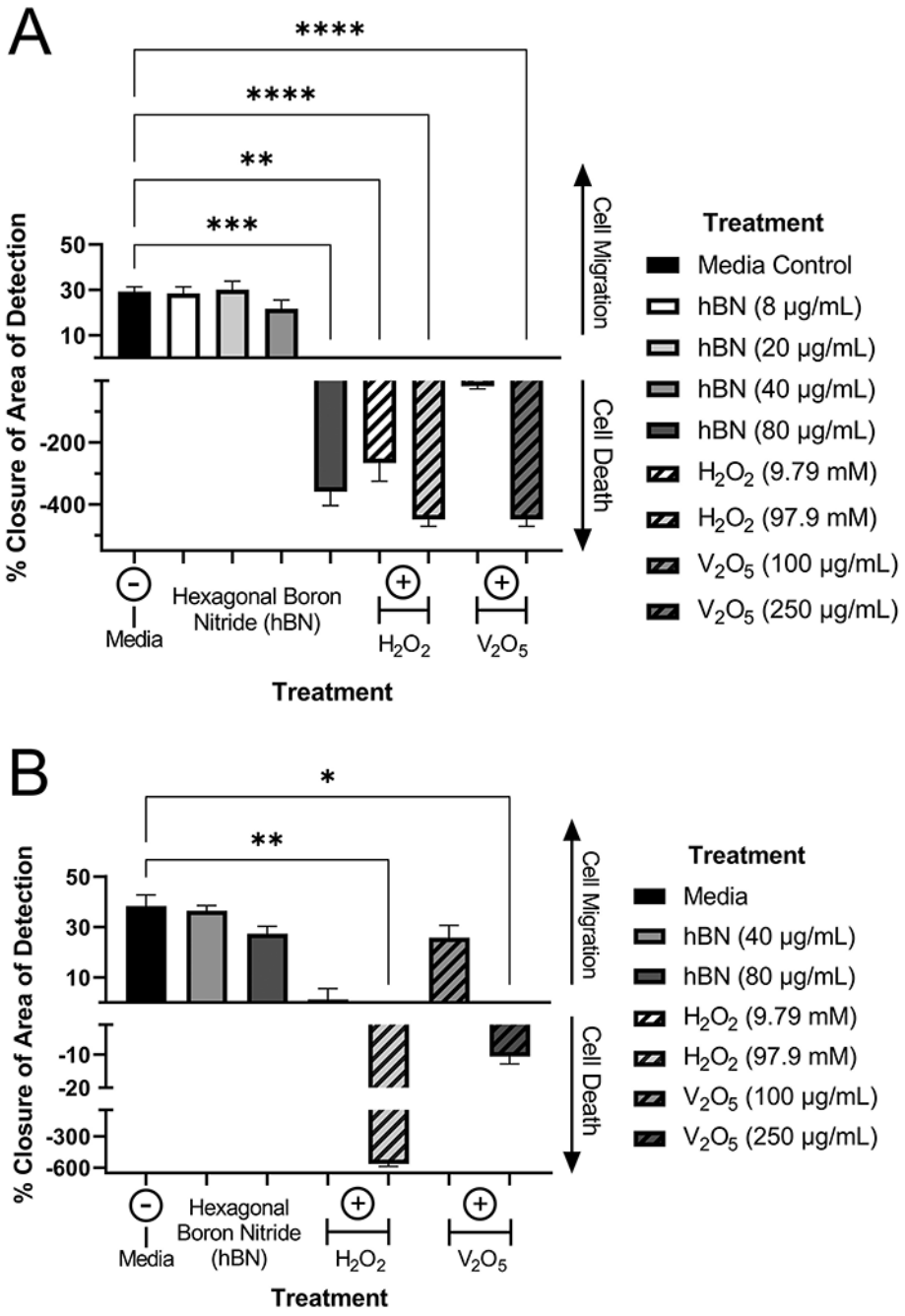

Fig. 5.

Cell migration (wound healing) following a dose response of hexagonal boron nitride (hBN) in human alveolar cell culture (A549) for either (A) 24-h continuous or (B) the initial 2 h of a 24-h time period. Sub-cytotoxic doses of hBN did not significantly inhibit wound healing at either exposure duration. Hydrogen peroxide (H_2O_2) and V_2O_5, a nanomaterial known to inhibit cellular migration, were used as positive controls. Kruskal-Wallis and Dunn's multiple comparisons tests were conducted: $^{**}P < 0.01$, $^{***}P < 0.001$, and $^{****}P < 0.0001$. For the 24-h exposure, N = 3 replicates (each an average of technical triplicates) for all

conditions. For the 2-h exposure, $N = 6$ media control, N = 3 for each positive control, and N = 6 (each an average of technical triplicates), for the hBN exposures.

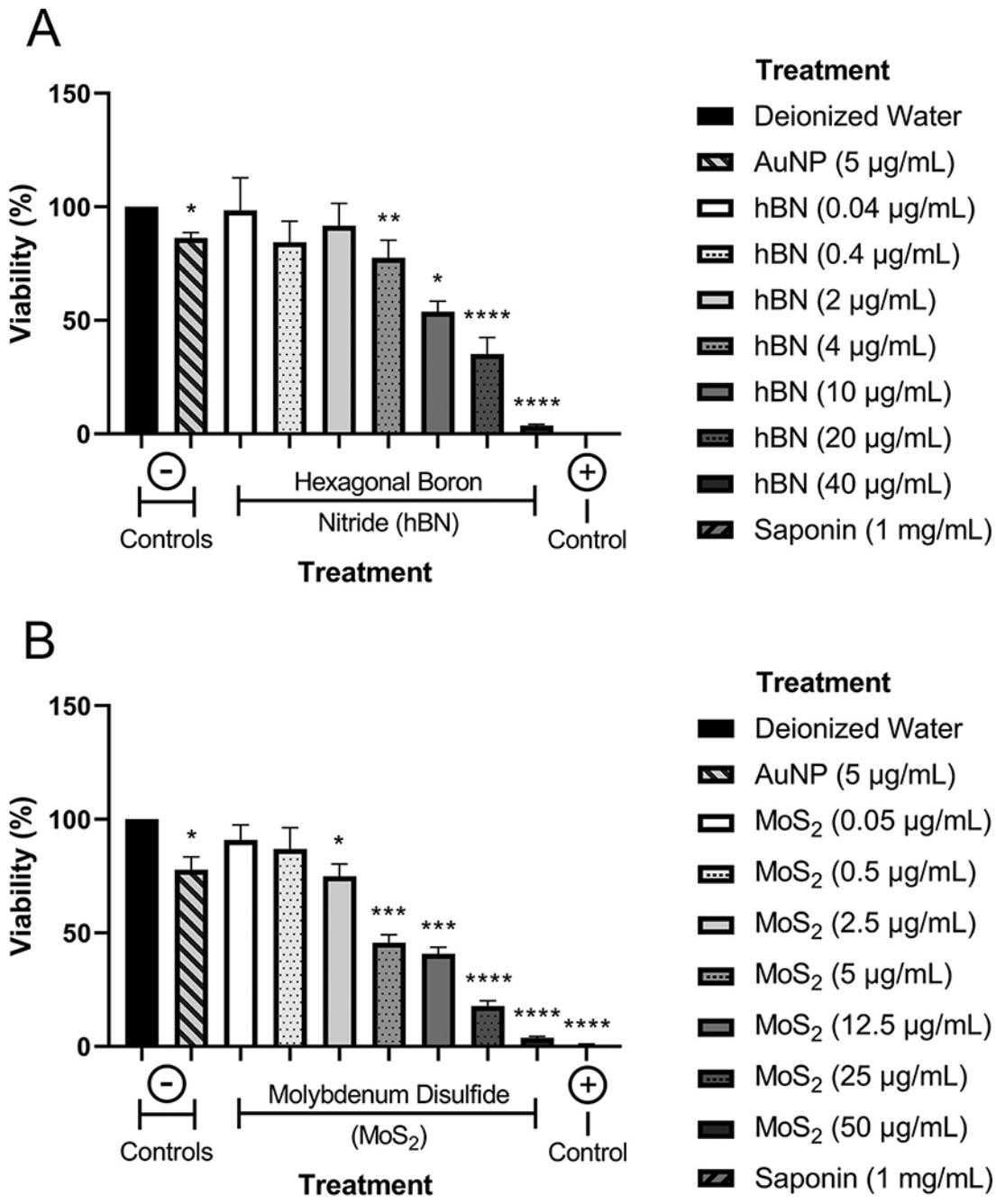

Fig. 6.

Cytotoxicity following a dose response of hexagonal boron nitride (hBN; A) and molybdenum disulfide (MoS_2; B) in human telomerase reverse transcriptase-immortalized corneal epithelial (hTCEpi) cells. Percent viability was measured by Calcein AM assay. Cytotoxicity of MoS_2 was induced from doses of 2.5 to 50 µg/mL, and cytotoxicity of hBN was induced from doses 4 to 40 µg/mL. Saponin and citrate-capped gold nanoparticles (AuNP) were used as a positive and negative control for cytotoxicity, respectively. An unpaired student's t-test with Welch's correction was performed to compare each treated

group to the media control group: *$P < 0.05$, **$P < 0.01$, ***$p < 0.001$, and ****$P < 0.0001$. N = 3 (hBN) or 4 (MoS_2) for all groups of that analysis. (For interpretation of the references to color in this figure legend, the reader is referred to the web version of this article.)

Table 1

General characteristics of the eight 2D nanomaterials utilized in this study.

Nanomaterial name	*Primary particle diameter*	Dispersion media	Dispersion concentration	Synthesis method
Graphene oxide	*400 nm* GO-400NMX400NM-DP20190115-1	Water	310 μg/mL	Improved Hummer's Method and Liquid-Phase Exfoliation
Reduced graphene oxide	*400 nm* RGO-400NMx400NM-DP04302018-1	Sodium cholate (3.88 mg/mL)	500 μg/mL	Modified Hummer's Method and Liquid-Phase Exfoliation
Graphene oxide	*250 nm* GO-250NMx250NM-DP20170315-1	Water	500 μg/mL	Improved Hummer's Method and Liquid-Phase Exfoliation
Graphene	*110 nm* G-110NMX110NM-DP20170315-1	Sodium cholate (5 mg/mL)	500 μg/mL	Liquid-phase Exfoliation
Reduced graphene oxide	*2 um* RGO-2μMX2μM-DP20190220-1	Sodium cholate (2.5 mg/mL)	400 μg/mL	Improved Hummer's Method and Liquid-Phase Exfoliation
Partially reduced graphene oxide	*400 nm* PRGO-400NMX400NM-DP20190630-1	Sodium cholate (4 mg/mL)	500 μg/mL	Improved Hummer's Method and Liquid-Phase Exfoliation
Hexagonal Boron Nitride	*150 nm* HBN-150NMX150NM-DP06252018-1	Sodium cholate (3.88 mg/mL)	402 μg/mL	Liquid-phase Exfoliation
Molybdenum disulfide	*400 nm* MOS2-400NMx400NM-DP08102018-1	Sodium cholate (5.17 mg/mL)	375 μg/mL	Liquid-phase Exfoliation